Neutron scattering study of the antiferroelectric transition in $TlD_2PO_4$



1998 J. Phys.: Condens. Matter 10 3045

(http://iopscience.iop.org/0953-8984/10/13/021)

J. Phys.: Condens. Matter **10** (1998) 3045–3060. Printed in the UK PII: S0953-8984(98)88717-1

# Neutron scattering study of the antiferroelectric transition in $TlD_2PO_4$

S Ríos†, M Quilichini† and J M Pérez-Mato‡

† Laboratoire Léon Brillouin, CEA-CNRS Saclay, 91191 Gif-sur-Yvette Cédex, France

‡ Departamento de Física de la Materia Condensada, Facultad de Ciencias, Universidad del País Vasco, Apdo 644, 48080 Bilbao, Spain

Received 27 October 1997

**Abstract.** The mechanism of the para–antiferroelectric phase transition at 353 K in $TlD_2PO_4$ has been investigated by coherent elastic and inelastic neutron scattering. The structural phase transition is shown to arise from the condensation of a diffusive mode to which a low-frequency zone boundary (at the S point $(\frac{1}{2}, \frac{1}{2}, 0)$) $S_1^+$ soft mode is coupled. The existence in $TlD_2PO_4$ of a weakly dispersive low-frequency optic branch along the $[\xi, \xi, 0]$ direction, which may be attributed to $PO_4$ rigid-body librations, may be regarded as an explanation of the appearance in the homologue $TlH_2PO_4$ of a pseudo–proper ferroelastic transition, already characterized by previous structural studies.

## 1. Introduction

In the present paper we report on the neutron scattering study concerning the mechanism of the para–antiferroelectric structural phase transition in $TlD_2PO_4$. This compound belongs to the family of (anti)ferroelectric materials of which $KH_2PO_4$ is known to be the prototype. One of the interests of this family of compounds resides on the large change that their static and dynamic properties show with deuteration: what is commonly known as the *isotope effects*. Many theoretical and experimental studies have been carried out in order to understand the causes of these effects, especially on the two prototype compounds: $KH_2PO_4$ for the ferroelectric compounds and $(NH_4)H_2PO_4$ for the antiferroelectric ones. For a long time, the difference in the tunnelling motion of protons and deuterons [1] was regarded as the origin of these effects. Nevertheless, a recent model [2] has been developed, in which isotope effects are shown to be caused by the isotope dependence of changes in the ground-state energy induced by a distortion of $PO_4$ tetrahedrons. The (anti)ferroelectric transitions observed in these compounds would thus be triggered by the strong coupling existing between the protons and the distortions of $PO_4$ groups.

The particular interest of the present study comes from the results of a recent accurate neutron diffraction study of the paraelectric ($T > T_c = 353$ K) [3] and the antiferroelectric (353 K $> T >$ 127 K) [4] phases of $TlD_2PO_4$. As reported in these works, despite having a isostructural high-temperature phase (hereafter called the *prototype phase*), $TlH_2PO_4$ and $TlD_2PO_4$ undergo two different types of structural phase transition when lowering the temperature. Thus, $TlD_2PO_4$ exhibits an antiferroelectric transition at 353 K from the prototype phase $Pbcn$ ($Z = 4$) to the monoclinic $P112_1/b$ ($Z = 8$) (see table 1). The order parameter has the $S_1^+$ symmetry with $\boldsymbol{q} = (\frac{1}{2}, \frac{1}{2}, 0)$. $TlH_2PO_4$, however, shows an intermediate ferroelastic phase not existing in $TlD_2PO_4$ between the prototype phase and

0953-8984/98/133045+16$19.50  

**Table 1.** Crystallographic data for $TlD_2PO_4$ above and below the transition temperature $T_c = 353$ K [3, 4]. The axis transformation between the orthorhombic (ort) and the monoclinic (mon) unit cells is as follows: $\boldsymbol{a}_{mon} = 2\boldsymbol{a}_{ort}$, $\boldsymbol{b}_{mon} = \boldsymbol{b}_{ort} - \boldsymbol{a}_{ort}$ and $\boldsymbol{c}_{mon} = \boldsymbol{c}_{ort}$.

| | Space group | Lattice parameters (Å,°) | | | | |
|---|---|---|---|---|---|---|
| | | $a$ | $b$ | $c$ | $\gamma$ | $Z$ |
| $T > T_c$ | $Pbcn$ | 4.535 | 14.36 | 6.556 | — | 4 |
| $T < T_c$ | $P112_1/b$ | 9.070 | 15.00 | 6.575 | 106.92 | 8 |

the antiferroelastic phase, which arises at 230 K. The ferroelastic transition in $TlH_2PO_4$, at 357 K, is from the prototype phase to the room-temperature monoclinic $P2_1/b11$ ($Z = 4$) phase. For this particular transition, the symmetry of the order parameter is $B_{3g}$ with $\boldsymbol{q} = 0$. The aim of this experimental work was twofold: first, to characterize the dynamics of the antiferroelectric phase in $TlD_2PO_4$, and second, to find a global interpretation of the two different structural phase transitions that $TlH_2PO_4$ and $TlD_2PO_4$ show when decreasing the temperature from the common prototype phase.

## 2. Structural properties of $TlD_2PO_4$

The important structural feature of $TlD_2PO_4$ is the 2D network of hydrogen bonds which links each phosphate group to the neighbouring ones forming layers parallel to the *ac* plane (see figure 1). The layers are connected to each other by the intercalated $Tl^+$ ions. Two crystallographically inequivalent hydrogen (deuterium) atoms, named hereafter $H_1$ ($D_1$) and $H_2$ ($D_2$), do exist in the structure. The first type of H (D) atom links $PO_4$ groups in zig-zag-like chains parallel to the *c* axis, while the second type links these chains along the *a* axis. In the prototype phase, both types of H (D) atom are disordered in a double-well potential along the hydrogen bond, whereas in the antiferroelectric phase they freeze into one of the two off-centre positions (see figure 2). Between the two types of deuterium atom, the $D_1$ type is considered to play the relevant role at the transition, as in the prototype phase the intrachain O–$D_1$–O bond distance (2.491 Å) is shorter than the interchain O–$D_2$–O distance (2.556 Å) [3]. Its behaviour is thus regarded as being more critical. The $D_2$ type are believed just to follow the $PO_4$ groups' motion. In the deuteron ordering process, one of the two crystallographic centres of inversion (the one in which $D_1$ type atoms are situated) is lost. Our structural study of the prototype phase has shown that the $PO_4$ tetrahedra may be considered as nearly perfect rigid groups, with a librational motion around the *a* axis. In the antiferroelectric phase, however, the ordering of deuterium atoms is accompanied by a strong distortion of $PO_4$ groups. The relative displacement of phosphorus atoms with respect to the surrounding oxygen atoms induces the appearance of a dipolar moment.

## 3. Experimental procedure

### *3.1. Samples*

Neutron elastic and inelastic measurements were carried out on single crystals of $TlD_2PO_4$, grown from a saturated solution of $TlD_2PO_4$ in heavy water by a slow-cooling process starting at 340 K. The deuteration degree is known to be higher than 98%. The crystals

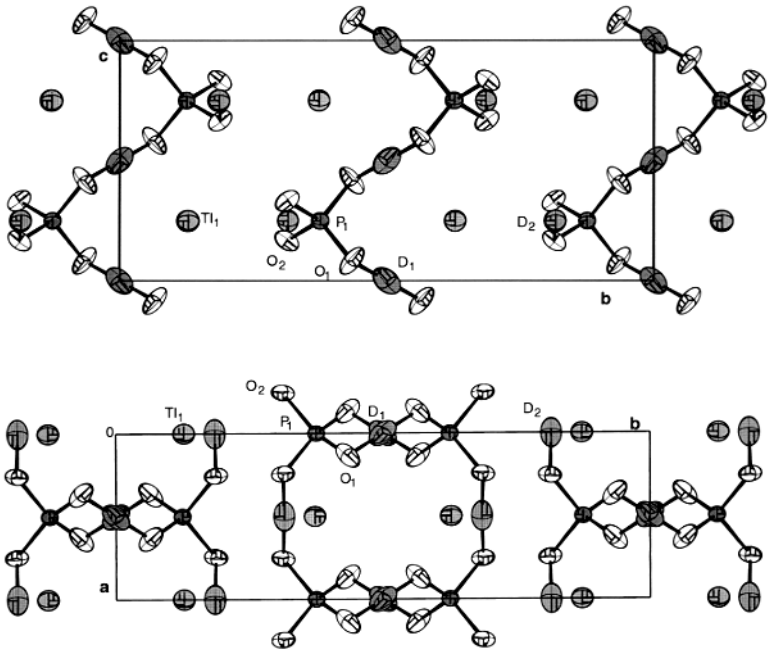


**Figure 1.** Two different projections of the structure of the prototype phase of $TlD_2PO_4$: above, along the [1, 0, 0] direction, and below, the [0, 0, 1] [4]. As the two off-centre positions of D atoms could not be precisely determined from structural data, these atoms have been situated at the centre of the O–O bonds.

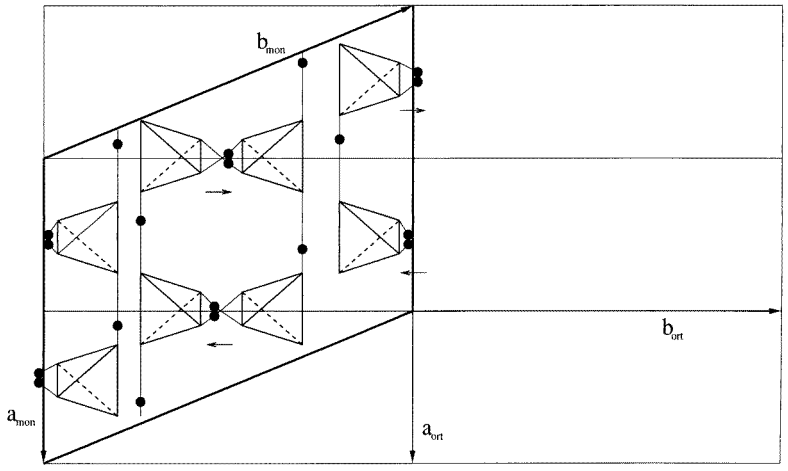


**Figure 2.** Projection of the orthorhombic and monoclinic unit cells on to the $0XY$ plane. The dots ● indicate the deuterium atoms, while $PO_4$ groups are indicated by tetrahedra. For more clarity thallium atoms have been omitted from the figure. Small arrows indicate the antiferroelectric ordering of $D_1$ type deuterium atoms.

were colourless, needle-shaped, and always twinned (growth twin), with the (021) as the twinning plane (indexation corresponding to the monoclinic system). For the measurements

reported here, one of the twins was removed by cutting the crystal along the twinning wall. The typical size of the samples was $3 \times 1 \times 0.5$ cm$^3$ (the longest direction being parallel to the $a$ axis), and the mosaic distribution of $\sim 0.25^\circ$. A series of experiments in the paraelectric phase has revealed that these crystals are very fragile when heated up above the transition, either for a long time or when going beyond 400 K. This is due to a chemical decomposition process which starts around these high temperatures. Therefore, the results reported in this paper were taken on several samples, and during the measurements the temperature of 400 K was never exceeded. In the antiferroelectric phase the superlattice reflections are Bragg peaks with no intrinsic width, but above the transition temperature a remaining diffuse scattering located at the position of the superlattice peaks was still observed. Then, we have determined the transition temperature as the temperature where we pass from the regime of superlattice Bragg reflections to the diffuse scattering one.

### *3.2. Instrumental details*

The measurements were undertaken on both 4F.1 and 4F.2 triple-axis spectrometers located on the cold-neutron beamline at the Reactor Orphée, Saclay (France). The study was carried out with a double monochromator of pyrolitic graphite and a flat analyser of the same material. An oriented graphite filter was used to remove order contamination in the incident 2.662 Å$^{-1}$ beam. Inelastic measurements were performed at fixed incident neutron energies of 8.05 meV ($k_i = 1.97$ Å$^{-1}$) and 5.58 meV ($k_i = 1.64$ Å$^{-1}$). For the elastic measurements a 14.70 meV (2.662 Å$^{-1}$) beam was used. The collimation was adjusted to meet the needs of the experiments; however, a constant $40'$ collimation was used after the sample and between analyser and detector. The crystals were always mounted inside an aluminium container, and subsequently in a standard furnace for triple-axis spectrometers in which the temperature stabilization was better than $\pm 0.1$ K. We have to point out that a temperature gradient between the thermocouple and the crystal was noticed, which was estimated to be 2–3 K. Within this shift determined transition temperatures were in agreement with the ones reported in the literature for the highly deuterated compound [5]. The crystal was always mounted with the $c$ axis perpendicular to the diffusion plane in order to study $(h/2, k/2, 0)$ superlattice reflections (the indexation hereafter will be always referred to the orthorhombic phase). As the best signal was obtained in the vicinity of the $(\frac{5}{2}, \frac{1}{2}, 0)$ superlattice reflection, most of the measurements were made around this reciprocal point. Even though the graphite filter is not completely effective for a 1.97 Å$^{-1}$ beam (around 15% of the intensity of the second harmonic is not filtered), in our case the order contamination was negligible due to the weak intensity of the (5 1 0) Bragg reflection; actually, at room temperature it is ten times less intense than the $(\frac{5}{2}, \frac{1}{2}, 0)$ superlattice reflection.

## 4. Elastic scattering results

### *4.1. Primary and secondary order parameters*

In antiferrodistortive structural phase transitions, and for small static displacements, the intensity of the superlattice reflections is proportional to the square of the order parameter, $\eta$. Figure 3 shows the integrated intensity of the $(\frac{5}{2}, \frac{1}{2}, 0)$ superlattice reflection. From the discontinuity of the intensity at the transition temperature, it is suggested to be a first-order, although close to a second-order transition. Considering Landau's theory for first-order transitions with zero cubic term, the intensity is expected to be described by the following

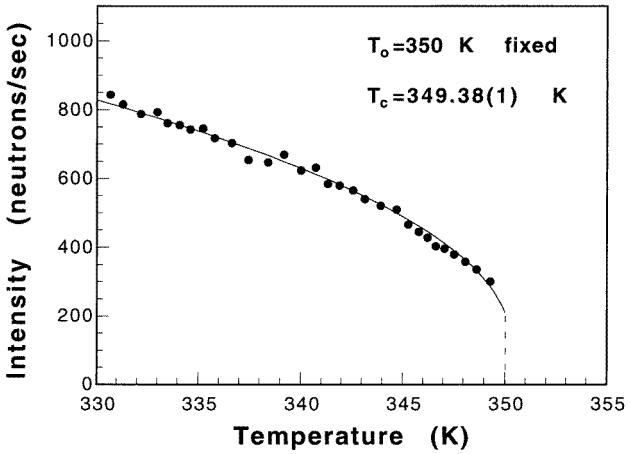


**Figure 3.** Temperature dependence of the intensity of the $(\frac{5}{2}, \frac{1}{2}, 0)$ superlattice reflection in $TlD_2PO_4$. Data have been fitted to (1).

expression [6]:

$$\eta^2 = \frac{2}{3}\eta_0^2\left[1 + \sqrt{1 - \frac{3}{4}\frac{T - T_c}{T_0 - T_c}}\right] \tag{1}$$

with $\eta_0 \equiv \eta(T = T_0)$, $T_c$ the limit of stability of the high-temperature phase and $T_0$ the transition temperature. Below $T_0$, the sample is composed of unknown fractions of antiferrodistortive domains, which may change with temperature. In our case, two kinds of domain were observed: those with the $(0, 1, 0)$ common plane. Figure 4 shows the relation between the $(h, k, 0)$ reciprocal plane of these two domains (named I and II). It may be seen how the superlattice reflections which are symmetry permitted (forbidden) in one domain are forbidden (permitted) in the order. Therefore, in our case the existence of domains did not influence the measurement of the superlattice intensity. The solid line in figure 3 is the result of a least-squares fit of our data to (1). $T_0$ and $\eta_0^2$ were fixed while $T_c$ was adjustable. The best fit was obtained for $T_c = 349.38(1)$ K when $T_0$ was fixed to 350 K. The small difference between $T_0$ and $T_c$ (close to the limit of our accuracy) indicates the nearly second-order character of the transitions, and thus, the proximity from a possible tricritical point. If taken as a continuous transition, the critical exponent of the primary order parameter is hence close to $\beta = 0.25$. A tricritical point had already been observed in $KH_2PO_4$ at 2 kbar pressure [7]. Attempts have been recently made in our laboratory to investigate the possible existence of a tricritical point in $TlD_2PO_4$, studying the superlattice reflection intensity as a function of the external pressure. Unfortunately, the crystal breaks around 1 kbar pressure. Although not completely established yet (powder diffraction measurements are in progress to clarify this point), the breaking should be associated with the para–antiferroelectric transition, and therefore, our result could be considered as an indication that in this crystal the first-order nature of the transition is enhanced with pressure. It is thus implied that the *possible* tricritical point if $TlD_2PO_4$ exists at pressures below atmospheric pressure, which is in agreement with the conclusions obtained by previous under pressure dielectric measurements [5] in relation with the antiferroelectric transition in $TlH_2PO_4$.

The spontaneous shear strain appearing at the transition has also been characterized by measuring its temperature dependence. We looked at the $(2, 0, 0)$ Bragg reflection, which

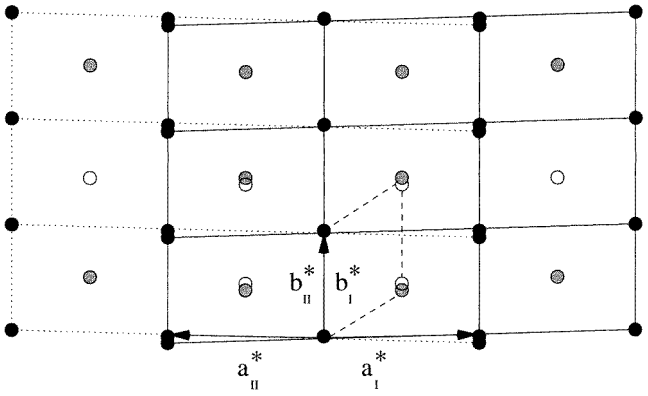


**Figure 4.** $(h, k, 0)$ reciprocal plane of the two twin domains (I solid lines and II dotted lines) observed in the antiferroelectric phase of $TlD_2PO_4$. $a^*$ and $b^*$ indicate the pseudo-orthorhombic cell. The monoclinic primitive cell is indicated by dashed lines. (●) represent Bragg reflections, and superlattice reflections are represented by white or grey circles depending whether they are symmetry permitted or forbidden, respectively.

splits into two parts in the antiferroelectric phase because of the existence of two types of orientational domain (the antiphase domains due to the loss of transitional symmetry cannot be observed by diffraction techniques). The angular separation of the two families of reflecting planes gave a measurement of the monoclinic shear strain $e_6$. Rocking curves were recorded by rotating the sample through the range of angles where the Bragg reflection $(2, 0, 0)$ took place. Figure 5(a) shows the measured rocking curves at three different temperatures. The spontaneous strain at each temperature was half of the distance between the two peaks. Very close to the transition temperature, our data were limited by the peak width determined by the crystal mosaicity. In antiferrodistortive crystals, any eventual spontaneous strain appears as a consequence of the linear–quadratic coupling between the strain and the order parameter. Hence, the strain is expected to be proportional to the square of the order parameter. However, as may be seen in figure 5(b) where we plot the square of the intensity (thus $\eta^4$) of the $(\frac{5}{2}, \frac{1}{2}, 0)$ superlattice reflection and the fourth power of the spontaneous strain, the spontaneous strain and the order parameter show a similar behaviour in temperature. This is an unusual behaviour, and we presume that it could be related to the tricritical nature shown by the order parameter.

### *4.2. Diffuse scattering*

The study of the temperature dependence of the superlattice reflection intensity revealed, above $T_0$, the existence of a diffuse scattering confined around these points. Therefore, detailed diffuse scattering measurements on the $(h\,k\,0)$ plane of $TlD_2PO_4$ were undertaken. In figure 6, we show two scans taken at the same temperature ($T_0 + 1.2$ K), in the vicinity of the $\boldsymbol{Q} = (\frac{5}{2}, \frac{1}{2}, 0)$ reciprocal lattice point, and along $a^*$ and $b^*$. These data were taken with an incident neutron energy of 14.70 meV (2.662 Å$^{-1}$), at zero energy transfer. It can be seen that the width of the scan along $h$ is nearly the instrumental resolution. From these measurements we can estimate an upper limit to the intrinsic width of 0.048(4) Å$^{-1}$ (FWHM), which corresponds to a correlation length inside the *ac* planes and along the *a* axis of $>42$ Å, or over nine chains. Nevertheless, for the scan along $k$ there is a significant broadening with respect to the instrumental resolution. After deconvolution a full width at

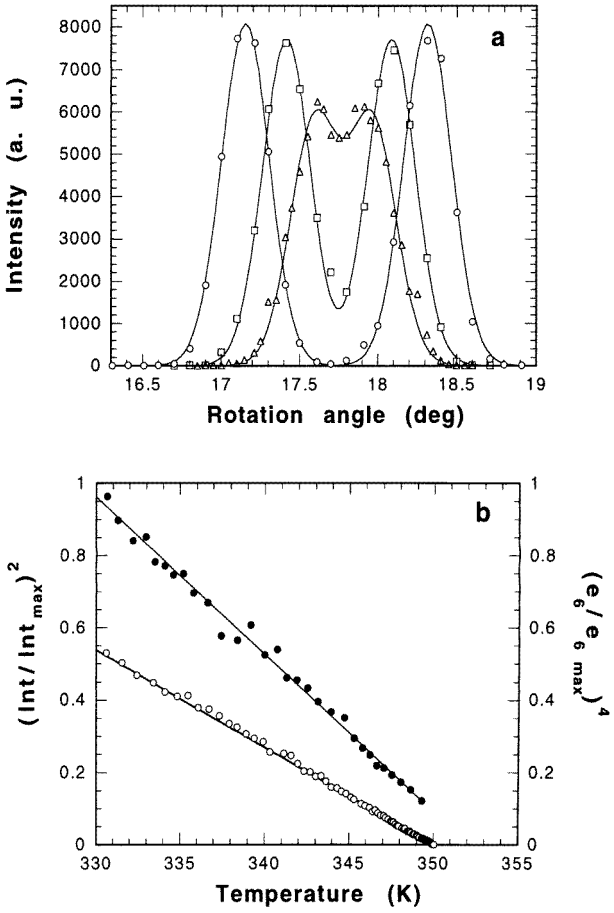


**Figure 5.** (a) Rocking curves obtained at three different temperatures around the $(2, 0, 0)$ Bragg reflection: (○) at 332 K, (□) at 348 K and (△) at 349.8(1) K. Measurements were undertaken at $k_i = 1.97$ Å. The intensity decay should be attributed to the increase in thermal vibration. (B) For comparison, we show the temperature dependence of the square of the intensity of the $(\frac{5}{2}, \frac{1}{2}, 0)$ superlattice reflection (●), and the fourth power of the spontaneous strain (○). Both have been first normalized to their maximum value.

half maximum of 0.123(6) $Å^{-1}$ was found. This corresponds to an interplane correlation of only 16 Å, i.e. just one cell. Attempts were made to measure the diffuse scattering out of the scattering plane, in the direction of the *c* axis, by tilting the crystal. Unfortunately, the vertical angular divergence of the outcoming beam does not allow us to estimate the real width, and subsequently the intrachain correlation length.

The temperature dependence of the peak width along the *b* direction, and therefore the interplane correlation length, was also studied. In figure 7 it can be seen how the interplane correlation only starts to develop at temperatures very close to the transition temperature, where the 3D character of the structure settles. Our results evidence the large anisotropy of the diffuse scattering in the prototype phase of $TlD_2PO_4$. The very weak correlation between the planes may be considered as another signature of the 2D character of the structure. For further studies it would be interesting to study in detail the temperature

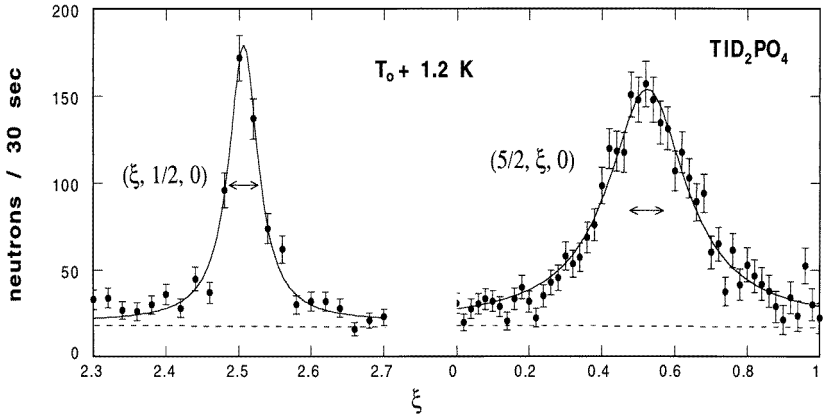


**Figure 6.** Observed scattering at the $Q = (\frac{5}{2}, \frac{1}{2}, 0)$ reciprocal lattice point. The scan on the left side is along $a^*$ and the scan on the right side is along $b^*$. Solid lines are the fits of the data to a Lorentzian function. The peak resolution (FWHM) was $\Delta_x = 0.0443$ Å$^{-1}$ and $\Delta_y = 0.0220$ Å$^{-1}$ respectively. It can be noticed that along $a^*$ the width is nearly limited by the instrumental resolution.

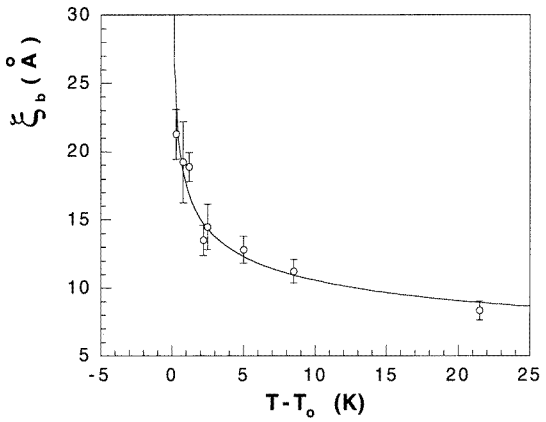


**Figure 7.** Temperature dependence of the correlation length, $\xi_b$, along the $b$ axis, i.e. between planes. The solid line is just a guide for the eyes.

dependence of the correlation lengths in the other two direction, along $a$ for the interchain correlation, and along $c$ for the intrachain correlation, and thus see whether the important feature of the structure is really two dimensionality, or whether the relevant fluctuations (the antiferroelectric fluctuations) triggering the transition have a one-dimensional nature and take place inside the chains parallel to the $c$ axis. The one-dimensional character of the diffuse scattering has also been observed in other compounds of the family, e.g. in the ferroelectrics $CsH_2PO_4$ and the deuterated homologue [8].

## 5. Inelastic scattering results

A study of the structural information given in figure 2 and table 1 reveals that the reduction in the transitional symmetry to pass from the paraelectric to the antiferrodistortive phase must

result from displacements modulated with the wave vector $\boldsymbol{q}_s = (\frac{1}{2}, \frac{1}{2}, 0)$ of the paraelectric phase (i.e. at the S zone boundary point). Table 2 gives the symmetry operations of the wave vector group, as well as the two bi-dimensional irreducible representations for this group, taken from [9]. Of the symmetry operations listed in table 2, only E, $C_{2z}$, $\sigma_z$ and I remain in the antiferroelectric phase. Thus, it can easily be demonstrated that the direction of the order parameter which produces the observed symmetry breaking corresponds to the (1, 1) direction of the bi-dimensional space of the order parameter, and thus, that the observed antiferroelectric phase in $TlD_2PO_4$ must be driven by an order parameter of symmetry $S_1^+$. Therefore, we have mainly studied the behaviour in temperature of the vibration modes of the paraelectric phase, above $T_0$, lying along symmetry lines in the $(h\,k\,0)$ plane and ending at the S point. In order to establish the nature of the instability leading to the phase transformation it has been sufficient to measure the low-frequency modes (up to 1 THz).

**Table 2.** Irreducible representations (irrep) of space group *Pbcn* at the S point $(\frac{1}{2}, \frac{1}{2}, 0)$, taken from [9]. The translations are: $\boldsymbol{t}_1 = \frac{1}{2}(\boldsymbol{a} + \boldsymbol{b})$, $\boldsymbol{t}_2 = \frac{1}{2}\boldsymbol{c}$ and $\boldsymbol{t}_3 = \frac{1}{2}(\boldsymbol{a} + \boldsymbol{b} + \boldsymbol{c})$.

| Irrep. | $\{E\|000\}$ | $\{C_{2x}\|\boldsymbol{t}_1\}$ | $\{C_{2y}\|\boldsymbol{t}_2\}$ | $\{C_{2z}\|\boldsymbol{t}_3\}$ | $\{I\|000\}$ | $\{\sigma_x\|\boldsymbol{t}_1\}$ | $\{\sigma_y\|\boldsymbol{t}_2\}$ | $\{\sigma_z\|\boldsymbol{t}_3\}$ |
|---|---|---|---|---|---|---|---|---|
| $S_1^+$ | $\begin{pmatrix}1&0\\0&1\end{pmatrix}$ | $\begin{pmatrix}0&\bar{1}\\1&0\end{pmatrix}$ | $\begin{pmatrix}\bar{1}&0\\0&1\end{pmatrix}$ | $\begin{pmatrix}0&\bar{1}\\\bar{1}&0\end{pmatrix}$ | $\begin{pmatrix}1&0\\0&1\end{pmatrix}$ | $\begin{pmatrix}0&\bar{1}\\1&0\end{pmatrix}$ | $\begin{pmatrix}0&\bar{1}\\\bar{1}&0\end{pmatrix}$ | $\begin{pmatrix}0&\bar{1}\\\bar{1}&0\end{pmatrix}$ |
| $S_1^-$ | $\begin{pmatrix}1&0\\0&1\end{pmatrix}$ | $\begin{pmatrix}0&\bar{1}\\1&0\end{pmatrix}$ | $\begin{pmatrix}\bar{1}&0\\0&1\end{pmatrix}$ | $\begin{pmatrix}0&\bar{1}\\\bar{1}&0\end{pmatrix}$ | $\begin{pmatrix}\bar{1}&0\\0&\bar{1}\end{pmatrix}$ | $\begin{pmatrix}0&1\\\bar{1}&0\end{pmatrix}$ | $\begin{pmatrix}1&0\\0&\bar{1}\end{pmatrix}$ | $\begin{pmatrix}0&1\\1&0\end{pmatrix}$ |

We have measured modes propagating along the $[\xi, \xi, 0]$ directions and $[0, \xi, 0]$ (with $0 \leqslant \xi \leqslant \frac{1}{2}$) and polarized in the $(a, b)$ plane, in the temperature range going from $T_0$ to 400 K. The Brillouin zones investigated were those centred at the Braggs positions (2, 1, 0) and (2, 0, 0). In the first one, the Bragg reflection (2, 1, 0) is symmetry forbidden, and therefore no acoustic mode is observed. In this zone we were able to evidence two low-energy optic modes. The corresponding branches along the $[\xi, \xi, 0]$ direction were revealed to be rather flat. The energy spectrum collected at the Brillouin zone boundary, shown in figure 8(a), evidences the existence of a quasi-elastic response centred at $\nu = 0$. The co-existence of a low-energy mode and the quasi-elastic scattering, together with the weak diffusive power of $TlD_2PO_4$ crystals, has made the data evaluation rather difficult. To fit the data, we have built a trial scattering function with a constant background, a sum of two damped harmonic oscillators (DHOs) for the phonon modes plus a Lorentzian and a Gaussian function centred at $\nu = 0$ to take into account the quasi-elastic scattering (when present) and the incoherent elastic scattering, respectively. This trial scattering function weighted with the Bose factor was folded with the instrumental resolution function. A least-squares fit of this scattering response to the data gave for each phonon mode the value of the adjustable parameters of the DHO, namely, the quasi-harmonic frequency, $\nu$, the damping constant, $\Gamma$, and the norm, $N_{ph}$, which is a quantity proportional to the inelastic structure factor of the mode. When a quasi-elastic signal was present in a given spectrum, the fit gave also the half width at half maximum (HWHM) and its norm $N_{Qs}$. During the fitting procedure we constrained the parameters of the Gaussian function describing the incoherent elastic scattering arising from the isotope distribution and nuclear spin. This was possible as the incoherent response could be measured independently, and its width has a value equal to the energy resolution of the spectrometer. The solid lines in figure 8(a, b) are the results of the best fit of the trail function to our data.

At $T_0 + 8$ K, the two optic modes have a quasi-harmonic frequency of $\nu_1 = 0.3$ THz and $\nu_2 = 0.5$ THz respectively. The upper frequency mode appears underdamped

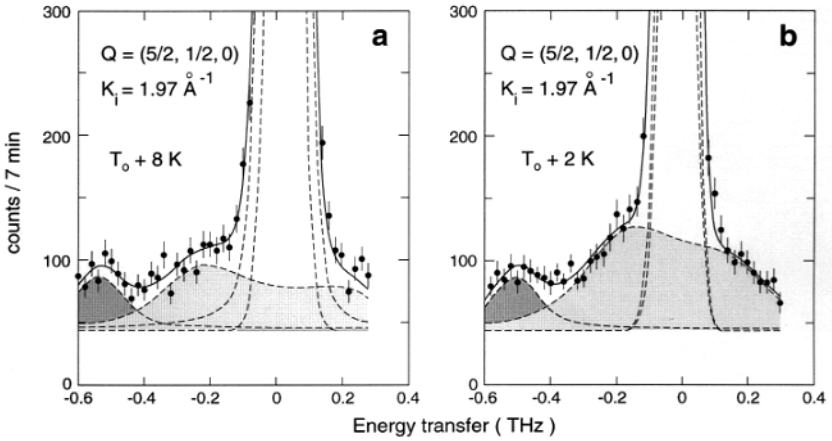


**Figure 8.** Energy profile of the inelastic scattering at a superlattice point in the paraelectric phase of $TlD_2PO_4$ at two different temperatures. The solid curves represent a least-squares fit to two damped harmonic oscillators and a Lorentzian function for the quasi-elastic scattering. The elastic incoherent scattering is described by an additional Gaussian with the instrumental resolution.

($\Gamma_2 = 0.12$ THz), while the lower one is broad ($\Gamma_1 = 0.3$ THz). The quasi-elastic response has a HWHM, 63 GHz, which is only slightly greater than the energy resolution (47 GHz for a constant $k_i = 1.97$ Å$^{-1}$). Along the $[\xi, \xi, 0]$ direction and out of the zone boundary, the quasi-elastic scattering does not exist and thus data could be analysed more easily. We have, then, been able to show that the lower optic mode remains broad all along this direction. In the second Brillouin zone, the Bragg $(2, 0, 0)$ has strong intensity which allows us to determine the dispersion of the acoustic modes emanating from it, propagating in the $[\xi, \xi, 0]$ direction and obviously polarized in the scattering plane. The $[\xi, \xi, 0]$ direction not being a high-symmetry direction, the detected acoustic modes are neither purely transverse not longitudinal; the purely transverse (polarized along $c$) not being seen in this geometry. For values of $\xi$ smaller than 0.2 in reduced units, these modes have no intrinsic width and are therefore true acoustic modes. For values of $\xi$ greater than 0.2 the two studied zones have given the same low-energy broad signal.

Along this direction, the modes being to one of the two irreducible representations $\Omega$ and $\Omega^-$ (symmetric and antisymmetric with respect to the $\sigma_z$ plane, respectively). The compatibility relations at the $\Gamma$ and S points are given in table 3. Unfortunately, the symmetry does not impose any restrictions on eigenvectors of normal modes propagating along this $[\xi, \xi, 0]$ direction, with the exception of the low values of $\xi$ for the acoustic modes. Let $TA_1$ be the acoustic mode polarized on the plane, and $TA_2$, the purely transverse polarized along the $c$ axis. Thus, $TA_1$, as the longitudinal acoustic mode, LA, belongs to the $\Omega$ representation and $TA_2$ to the antisymmetric $\Omega^-$. As we shall explain in detail later on, the lower optic phonon is of $\Omega^-$ symmetry, and then, there has to be an anticrossing process between this latter mode and the $TA_2$ acoustic mode, at $\sim$0.2, where the widths of the phonon modes have been exchanged. The sound speeds (and elastic constants C) determined from our measurements were: $v_L = 712$ m s$^{-1}$ ($C = 2.3 \times 10^9$ N m$^{-2}$, with $\varrho = 4.51$ g cm$^{-3}$) and $v_T = 1340$ m s$^{-1}$ ($C = 8.1 \times 10^9$ N m$^{-2}$). From the small values obtained for this direction of propagation, it may be deduced that the structure of $TlD_2PO_4$ is rather soft.

A partial determination of the symmetry of the measured optic modes can be done using the extinction rules for inelastic neutron scattering, whose existence has been recently pointed out [10]. In general terms, a mode of symmetry $\tau$ and wave vector $\boldsymbol{q}$ is to be active at a scattering vector $\boldsymbol{Q}$, if and only if the identity representation is contained in the representation (of the $Q$-invariant point group, $P_Q$) defined as:

$$T(R) = \tau^*((R, \boldsymbol{t}))e^{i\boldsymbol{Q}\cdot\boldsymbol{t}} \tag{2}$$

where $R$ is any operation belonging to $P_Q$ and $\tau^*((R, t))$ is the complex conjugate of the operator associated with the space group operation $(R, t)$ by the small representation $\tau$. This general rule applied to our case implies that all modes with wave vector in the plane $l = 0$ and detected in the Brillouin zone $(2, 1, 0)$ should be antisymmetric for the mirror plane $\sigma_z$, hence of symmetry $A_u$, $B_{1u}$, $B_{2g}$ or $B_{3g}$ at the $\Gamma$ point, and $\Omega^-$ along the direction $[\xi, \xi, 0]$. Conversely, the modes measured in the Brillouin zone $(2, 0, 0)$ are necessarily symmetric for the same mirror plane, i.e. of symmetry $A_g$, $B_{1g}$, $B_{2u}$ or $B_{3u}$ or $\boldsymbol{q} = \boldsymbol{0}$, and $\Omega$ along the direction $[\xi, \xi, 0]$. For the modes at the zone border $(\frac{1}{2}, \frac{1}{2}, 0)$ no selection rule exists, in agreement with the fact that this point is common to both Brillouin zones. These symmetry arguments are also consistent with the compatibility relations of table 3.

**Table 3.** Compatibility relations between the $\Gamma$ point and S point $(\frac{1}{2}, \frac{1}{2}, 0)$ along the $[\xi, \xi, 0]$ direction. Since in an orthorhombic primitive unit cell the two irreducible representations in the $(h\,k\,0)$ plane do not have any specific name, we have arbitrarily decided to name them $\Omega$ and $\Omega^-$, symmetric and antisymmetric with respect to the plane, respectively. The irreducible representations at the $\Gamma$ point are all one dimensional, whereas in the plane and at the S point they are doubly degenerate.

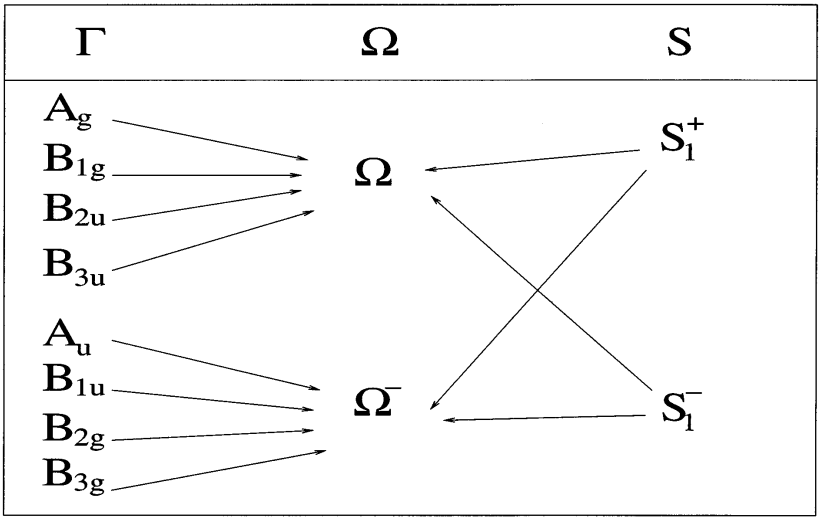


Taking into account all these considerations, an approximate scheme for the dispersion curves at $T_0 + 1$ K corresponding to our measurements along the $[\xi, \xi, 0]$ direction is proposed in figure 9. Given the scarce data, the scheme is quite speculative for the higher branches. We know from Raman measurements [11] that a large number of branches are present in $TlD_2PO_4$ with frequencies around 1 THz, and therefore the scheme might be much more complicated in this region. In fact, at $\xi = 0.3$, according to the figure, a single branch is being apparently detected in both geometries, a fact which cannot be reconciled with the

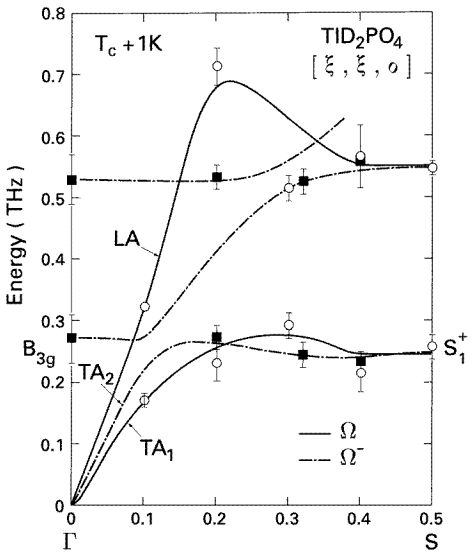


**Figure 9.** Proposed dispersion curves of the low-frequency modes of $TlD_2PO_4$ at 1 K above the transition temperature and along the $[\xi, \xi, 0]$ direction of the reciprocal space. Experimental points indicated by (■) and (○) were taken in the $(2, 1, 0)$ and $(2, 0, 0)$ Brillouin zones, respectively. Solid lines are just a guide for the eyes.

extinction rules discussed above, unless an additional branch is added. The labelling of the lowest mode at the Brillouin zone border as $S_1^+$ comes naturally from the observation of its significant softening when approaching $T_0$ (explained below), which indicates that its symmetry is identical to that of the order parameter. The choice of $B_{3g}$ for the first optic mode at the Brillouin zone centre is a consequence of the following considerations. According to our diffraction results [4], this optic mode could be attributed to the $PO_4$ rigid-body libration around the orthorhombic *a* axis. Concerning the symmetry properties of this librational motion, as the site symmetry of the $PO_4$ group is $C_{2y}$, it has a B symmetry (following the notation of Bradley and Cracknell [12]), which induces in the crystal normal modes belonging to the $B_{1g}$, $B_{1u}$, $B_{3g}$ and $B_{3u}$ irreducible representations of the factor group of the crystal. Therefore, we know that the symmetry at $\boldsymbol{q} = \mathbf{0}$ of this librational mode should be either $B_{1u}$ or $B_{3g}$. As the symmetry of the order parameter for the intermediate phase of the non-deuterated compound $TlH_2PO_4$ is $B_{3g}$, this last symmetry should be taken as the most plausible from the two. This mode, however, has not been observed in the previously mentioned Raman scattering study, probably because the measurements were carried out on powder samples and also because of the low polarizability of $PO_4$ ions. Nevertheless, there exists in the low-frequency range of the Raman spectra a strong and broad signal which has not been analysed and it precludes the observation of a low-energy mode. To be complete let us say that our second optic mode (the upper one) reported above corresponds to the lowest mode observed in the mentioned Raman scattering study.

In the next paragraphs we shall report the temperature dependence of both low-energy modes and the quasi-elastic scattering as the temperature $T_0$ is approached from above. One run at 300 K, in the antiferroelectric phase, was also undertaken.

Above $T_0$, we have observed that the upper mode is not sensitive to the temperature variation, and therefore, we think that it is not directly implicated in the phase transition. The

lower branch however softens slightly (see figure 8(b)) close to $T_0$, for $T_0 < T < T_0 + 2$ K, while its damping remains constant within the accuracy of our measurements. These two optic modes were also measured at room temperature. Figure 10 shows these modes at $\boldsymbol{q} = \mathbf{0}$ at the Bragg $(1, 4, 0)$ and at the superlattice $(\frac{3}{2}, \frac{7}{2}, 0)$ positions, respectively. From these spectra we may see that the lower-energy mode has renormalized to a quasi-harmonic frequency of 0.4 THz and now it is underdamped with $\Gamma_1 = 0.12$ THz, while the upper mode is still unchanged; its frequency has only slightly increased, as expected when the temperature is decreased.

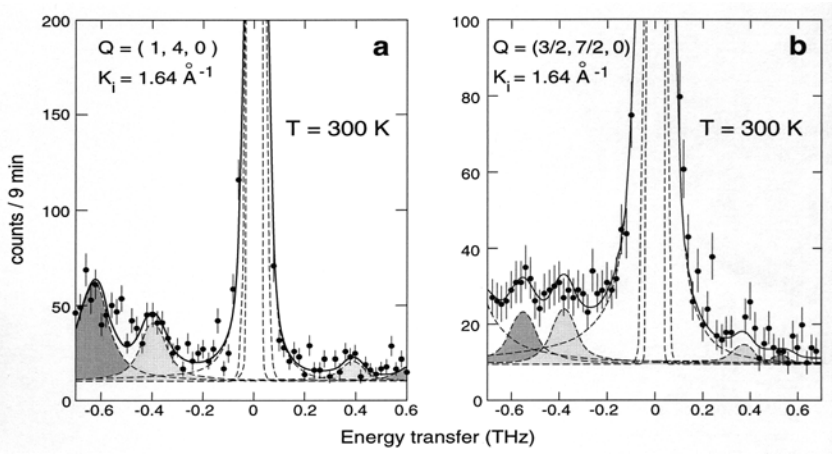


**Figure 10.** Energy profiles taken at the Γ point of the antiferroelectric phase (at 300 K) of $TlD_2PO_4$: (a) at the $(1, 4, 0)$ Bragg reflection and (b) at the $(\frac{3}{2}, \frac{7}{2}, 0)$ superlattice reflection. The solid lines correspond to the result of the fitting process of our data to the sum of two damped oscillators and two Gaussian functions to take into account the incoherent elastic scattering and the Bragg contamination at $\nu = 0$. It was also necessary to use a Lorentzian function to evaluate the contamination coming from the acoustic modes.

The quasi-elastic scattering observed above $T_0$ around the $(\frac{5}{2}, \frac{1}{2}, 0)$ point, shown to be $\xi$ dependent along the $[0, \xi, 0]$ direction, where the diffuse scattering described above has the larger width, and as expected as $\xi$ increases along $[0, \xi, 0]$, the width of the signal increases and the intensity decreases. Moreover, it has an increasing intensity as the temperature is lowered to $T_0$. More specifically, figure 11 shows the results obtained at three different temperatures at $\boldsymbol{Q} = (\frac{5}{2}, \frac{1}{2}, 0)$. The incoherent elastic scattering has already been subtracted from the measured spectra, after having been measured independently at each temperature. The spread in energy of the quasi-elastic scattering does not show any significant increase in width with respect to the instrumental resolution. Thus, the antiferroelectric fluctuations in $TlD_2PO_4$ occur on a time scale higher than $2 \times 10^{-11}$ s.

## 6. Discussion

In the foregoing, we have evidenced a soft overdamped libration branch of $PO_4$ rigid-body groups (of $\Omega^-$ symmetry) and the condensation of a relaxational mode at the S point of the orthorhombic Brillouin zone. This relaxational mode should be associated, following the adiabatic approximation developed by Sugimoto and Ikeda [2], to a cooperative motion where the hopping of deuterons are induced by the ordering of the dipole moments. These dipole moments appear as a consequence of the internal distortion of $PO_4$ groups. On

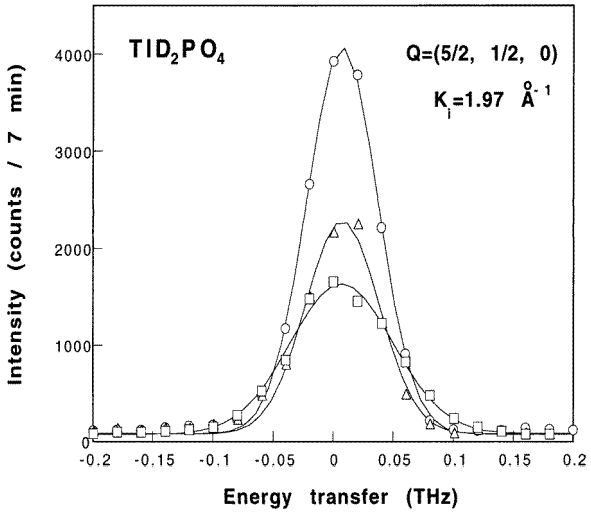


**Figure 11.** Temperature dependence of the quasi-elastic scattering at the superlattice point $\boldsymbol{Q} = (\frac{5}{2}, \frac{1}{2}, 0)$: at $T_0 + 21$ K (□), $T_0 + 2.5$ K (△) and $T_0 + 1.2$ K (○).

the other hand, and regarding the ratio between the flipping rate of D–$PO_4$ groups ($\tau > 2 \times 10^{-11}$) and the quasi-harmonic frequency of the soft librational phonon ($\nu \sim 0.3$ THz), and in the frame of a spin–phonon coupling, we may say that our system falls in the slow relaxation regime, where $\nu > \tau^{-1}$. That is, is mainly the order–disorder character of the pretransitional fluctuations which triggers the transition. The signature of the coupling between the two modes appears in the width of the soft phonon.

If we compare our results to those obtained in $KH_2PO_4$, we see that the existence at low frequencies of both a $PO_4$ librational mode [13] and a relaxational mode [14] has already been reported. Nevertheless, a significant shift is noticed between the frequencies of these two modes when comparing $KH_2PO_4$ and $TlD_2PO_4$. While in $KH_2PO_4$ Raman scattering measurements observe the librational mode at $\sim$150 $cm^{-1}$ (4.5 THz) and the relaxational mode below 20 $cm^{-1}$ (0.6 THz), in $TlD_2PO_4$ we find both at frequencies around fifteen times lower, respectively. This shift might be explained regarding the lattice modifications induced by the substitution of the light $K^+$ ion by the much heavier $Tl^+$.

Another argument which favours the hypothesis of attributing the lower optic branch to a $PO_4$ rigid-body libration motion may be found when looking at the homologue $TlH_2PO_4$. As said in the introduction, the prototype phase in $TlH_2PO_4$ is unstable at 357 K (nearly the same transition temperature as the one observed in $TlD_2PO_4$), but nevertheless, the type of structural transition observed is rather different. As Brillouin scattering [15] and ultrasonic [16] measurements clearly showed, the transition in $TlH_2PO_4$ is ferrodistortive. Furthermore, at this transition the ordering of hydrogen bonds is not complete (only $H_2$ atoms are ordered), and what is more important, the atomic displacement field evidences the condensation of a $PO_4$ rigid-body libration with the same symmetry as the order parameter, i.e. $B_{3g}$ [4]. Thus a low-frequency librational optic mode of $B_{3g}$ symmetry at $\boldsymbol{q} = \boldsymbol{0}$ would be expected to exist in $TlH_2PO_4$, and to show a soft behaviour. So far, no Raman or neutron scattering measurements concerning this particular phase transition of $TlH_2PO_4$ have been reported yet. We think, therefore, that a Raman scattering study of the low-frequency modes of $TlH_2PO_4$ would be very interesting, emphasizing more specifically the possible softening

of a $B_{3g}$ mode. Our results showing the existence in $TlD_2PO_4$ of a low-frequency branch of which the symmetry at $\boldsymbol{q} = \mathbf{0}$ might be $B_{3g}$ (our study is not able to discriminate between $B_{3g}$ and $B_{1u}$) may be regarded as a motivation for such an experiment.

If future Raman or neutron scattering experiments in $TlH_2PO_4$ confirm the existence of a low-frequency $B_{3g}$ symmetry mode, a qualitative global interpretation of the two phase transitions observed in $TlH_2PO_4$ (at 357 K) and in $TlD_2PO_4$ (at 353 K) could be the following. Regarding the structure of the prototype phase, the libration of $PO_4$ groups might be considered as an unstable degree of freedom. Since in the ferroelastic phase of $TlH_2PO_4$, $H_1$ atoms are still disordered and $PO_4$ groups are just slightly distorted, it is expected to observe at 357 K the freezing of the relaxational mode associated to $H_1$ type atoms (it would only take place at the transition at 230 K, when $H_2$ atoms are ordered) and therefore, the only mode involved in the transition would be the librational mode. This mode, coupled to the spontaneous shear strain (of $B_{3g}$ symmetry) would trigger the observed ferroelastic transitional. For $TlD_2PO_4$, however, the condensation of the relaxational mode associated to $D_1$ type atoms is observed at 353 K (as reported in this paper), and, as a consequence of the spin–phonon coupling, the librational mode softens at the transition.

We would like finally to stress that all through this argumentation, $H_2$ ($D_2$) type atoms have not been taken at all into account. Although there is no direct evidence, apart from that derived from the structural analysis, we think that they play no relevant role in the mentioned structural phase transitions. In fact, since the O–$H_2$ ($D_2$)–O bond lengths are longer than O–$H_1$ ($D_1$)–O bonds, we wonder whether $H_2$ ($D_2$) atoms are really disordered in a double-well potential, or if the potential shape looks more like an anharmonic single potential. In this case, their motion would be less critical regarding the factors which trigger the observed phase transitions. The critical fluctuations in $TlH_2PO_4$ and $TlD_2PO_4$ would take place inside the O–$H_1$ ($D_1$)–O arrangements, and these compounds might be thus considered as one-dimensional systems from the point of view of the hydrogen ordering, e.g. $CsH_2PO_4$. Nevertheless, we should remind the reader that, in this latter compound, deuteration does not seem to induce such important effects as those observed in the $TlH_2PO_4/TlD_2PO_4$ system regarding their two different phase transition sequences.

## 7. Concluding remarks

Using neutron scattering techniques we have investigated the mechanism of the antiferroelectric transition in $TlD_2PO_4$. It is clear that although the transition is mainly of order–disorder type, there is also a weakly soft mode which evidences the displacive character of the transition. Nevertheless, further studies are still needed to establish the dimensionality (2D or 1D) of the antiferroelectric fluctuations in this system.

## Acknowledgments

We are grateful to J M Godard for growing the single crystals used in our experiments. One of the authors (SR) would also like to thank the Department for Research of the Basque Government for the financial support.

## References

[1] Blinc R 1960 *J. Phys. Chem. Solids* **13** 204
[2] Sugimoto H and Ikeda S 1991 *Phys. Rev. Lett.* **67** 1306
[3] Ríos S, Paulus W, Cousson A, Quilichini M, Heger G, Pasquier B and Le Calvé N 1995 *J. Physique* I **5** 763

[4] Ríos S, Paulus W, Cousson A, Quilichini M and Heger G 1998 *Acta Cryst.* B accepted
[5] Yasuda N, Fujimoto S, Asano T, Yoshino K and Inuishi Y 1980 *J. Phys. D: Appl. Phys.* **13** 85
[6] Dorner B, Axe J D and Shirane G 1972 *Phys. Rev.* B **6** 1950
[7] Schmidt V H, Western A B and Baker A G 1976 *Phys. Rev. Lett.* **37** 839
[8] Frazer B C, Semmingsen D, Ellenson W D and Shirane G 1979 *Phys. Rev.* B **20** 2745
[9] Stokes H T and Hatch D M 1988 *Isotropy Subgroups of the 230 Crystallographic Space Groups* (Singapore: World Scientific)
[10] Pérez-Mato J M, Hlinka J, Aroyo M, Quilichini M and Currat R *Phys. Rev. Lett.* submitted
[11] Pasquier B, Le Calvé N, Al-Homsi-Teiar S and Fillaux F 1993 *Chem. Phys.* **171** 203
[12] Bradley C J and Cracknell A P 1972 *The Mathematical Theory of Symmetry in Solids* (Oxford: Clarendon)
[13] Tominaga Y, Urabe H and Tokunaga M 1983 *Solid State Commun.* **48** 265
[14] Tominaga Y and Urabe H 1982 *Solid State Commun.* **41** 561
[15] Arai M, Yagi T, Sakai A, Komukae M, Osaka T and Makita Y 1990 *J. Phys. Soc. Japan* **59** 1285
[16] Hanazawa K, Komukae M, Osaka T, Makita Y, Arai M, Yagi T and Sakai A 1991 *J. Phys. Soc. Japan* **60** 188